33A.0 IN-SITU STUDIES OF STRAIN RATE EFFECTS ON PHASE TRANSFORMATIONS AND MICROSTRUCTURAL EVOLUTION IN BETA-TITANIUM ALLOYS (LEVERAGED)

Benjamin Ellyson (Mines)
Faculty: Amy Clarke (Mines)
Other Participants: Jonah Klemm-Toole (Mines), Michael Kaufman (Mines), Robert Field (Mines)
Industrial Mentor: Austin Mann (Boeing), Clarissa Yablinski (LANL), John Foltz (ATI)

This project initiated in Fall 2017 and is supported by the Office of Naval Research (ONR). The research performed during this project will serve as the basis for a Ph.D. thesis program for Benjamin Ellyson.

33A.1 Project Overview and Industrial Relevance

Titanium alloys are heavily used in the aerospace and biomedical industries for their high specific strength and good corrosion resistance. However, low work hardening rates and uniform elongation have limited their applicability in deformation controlled applications, where high energy absorption or good formability are required. The ability to develop novel titanium alloys that exhibit high work hardening rates would broaden their applicability, for lightweight, blast-resistant armor, crash resistant structural components, and high-complexity plastically formed parts, for example. Recent work [33.1-33.4] on metastable β-titanium alloys has shown promising results, wherein high work hardening rates and uniform elongations were achieved through TRansformation Induced Plasticity (TRIP) and TWinning Induced Plasticity (TWIP). These deformation mechanisms have been the subject of extensive study in ferrous alloys, while published work in other alloy systems, especially body centered cubic (BCC) alloys, is limited in scope. The present project aims to study TRIP and TWIP effects in β-titanium to garner fundamental understanding of the intrinsic and extrinsic variables controlling TRIP and TWIP. The fundamental knowledge gained from this study will be used to develop an alloy design methodology that will enable tailoring of microstructural evolution, deformation mechanisms, and mechanical response by means of alloying and processing.

33A.2 Previous Work

The previous reporting cycle was mostly aimed at preparing and executing in-situ synchrotron experiments. Beamtime was allocated at Sector 32-ID at the Advanced Photon Source (APS) in February 2020 and the Cornell High-Energy Synchrotron Source (CHESS) in March 2020. The APS experiments involving pressure bar tensile testing at strain rates of ~10^3 s^{-1} were successfully completed, while CHESS experiments were postponed, due to the COVID-19 pandemic. **Table 33.1** lists the experimental matrix tested during the APS experiments. Intermediate tensile testing at strain rates of 10^{-1} and 10^0 s^{-1} was also performed at Mines. Transmission electron microscopy (TEM) characterization of the fine-scale microstructure details in the alloys Ti-1023 and Ti-15Mo after deformation in tension at quasi-static strain rates was also pursued in the last reporting period.

33A.3 Recent Progress

33A.3.1 APS Dynamic In-situ Data and Post-Mortem Characterization

The APS high-rate tensile testing experiments conducted in February 2020 allowed for the simultaneous collection of time-resolved mechanical, diffraction and radiography data during deformation, as schematically shown in **Figure 33.1**. Analysis of the in-situ imaging and diffraction data during pressure bar testing and post-mortem microstructure characterization has progressed during the last reporting period. Post-processing of the diffraction data has yielded promising results, with strong evidence for transformation or twinning found for almost every alloy and heat treatment. Indeed, the heat treatments indicated in **Table 33.1** exhibited the expected microstructural evolution. **Figure 33.2** shows an integrated diffraction pattern taken during tensile deformation of an as-quenched Ti-1023 specimen at a strain rate of 10^3 s^{-1}. These data clearly show the appearance of new diffraction peaks associated with the formation of martensite (intensity near the green lines), and the corresponding decrease in intensity of the β-phase peak (intensity near the black line). Diffraction data seem to indicate that the structure of the β phase and α" martensite is similar to that obtained after deformation under quasi-static conditions. Although perfect alignment of the predicted and measured peaks is not obtained. Electron backscatter diffraction (EBSD) and TEM post-mortem characterization of the deformed samples are currently underway. Post-mortem EBSD of the Ti-

Mo binary solid solutions has been completed and is underway for the Ti-1023 specimens. **Figure 33.3** shows the inverse pole figure (IPF) map of an EBSD scan from the gage section of a Ti-15Mo specimen deformed in tension at a strain rate of 10^3 s^{-1}. **Figure 33.4** shows an image quality (IQ) map, wherein the twin boundaries have been highlighted by color, based upon the twinning system. Ti-15Mo is known to be TWIP dominant when an equiaxed β phase microstructure is deformed at quasi-static strain rates, deforming exclusively by {332}<113> twinning and slip. Surprisingly, the more conventional {112}<111> BCC deformation twinning system can also be seen, highlighted in green as secondary twinning product inside of primary {332} twinning (**Figure 33.4**). While activation of secondary {112} twinning has been reported in certain TWIP Ti alloys at quasi-static strain rates, this has never been reported before in Ti-15Mo, as it is usually associated with alloys with higher β phase chemical stability. These results seem to indicate that an increase in strain rate has intrinsically affected the phase stability and microstructural evolution.

Bands showing extremely fine and complex microstructural evolution can be seen in **Figure 33.3** that seem to indicate either severe grain refinement, or the onset of shear banding that will require further fine-scale characterization in the near future. Many large primary twins also show a fine-scale evolution of secondary product. These complex hierarchical twin bands indicate that TWIP remains an effective means to alleviate plastic strain localization and prohibit local instability, even during deformation at high strain rate.

Two publications are currently in preparation for this segment of the project. One will be focused on the comparison of high-strain rate tensile deformation of two different chemistries in the Ti-Mo binary system to elucidate the effect of β phase chemical stability on microstructural evolution at high strain rate. The second will be focused on the interaction of low-temperature aging and high-strain rate testing on microstructural evolution in Ti-1023 aged to various degrees.

33A.3.2 Quasi-Static Tensile Deformation of Aged Ti-1023

Transmission electron microscopy (TEM) from previous reports revealed that low-temperature aging of Ti-1023 causes coarsening of athermal ω precipitates formed in the β matrix during quenching from the β phase field (above 1123 K for Ti-1023). Recent EBSD characterization of interrupted tensile tests of low-temperature aged Ti-1023 has revealed microstructural evolution dominated by martensite produced by TRIP. **Figure 33.5** shows that microstructural evolution occurs by TRIP in the as-quenched and 900 s, 423 K (150 °C) aged condition, also referred to as the max TRIP stress condition or MTS. TEM characterization of deformed material in the MTS condition seems to confirm this finding. However, these same TEM data show evidence of nano-scale β phase deformation bands, which are suspected of being deformation twins. Literature also supports the possibility of these bands being formed upon unloading, when α" martensite reverts to β phase, which can leave behind deformation bands with or without a twinning relationship to the initial matrix, depending on the variant selected during loading. Further TEM characterization is necessary to prove whether a twining relationship exists between the bands and the matrix and the origin of these bands (loading or reversion twins). EBSD and TEM characterization support the finding that deformation is still largely TRIP dominant up to aging times of roughly 1800 s at 423 K. Further aging treatments at 423 K (150 °C) were conducted to elucidate the transition to a TRIP-inhibited (TI) condition (7200 s of aging at 423 K). The TI condition is characterized by a complete suppression of TRIP during deformation, which is replaced by dislocation slip that is localized in narrow bands or "channels". This heterogeneous slip deformation causes a concentration of plasticity which leads to low work hardening and strongly reduces ductility. Further aging treatments were investigated to understand the transition from the MTS to the TI condition. Aging times of 1800 s and 2700 s at 423 K were performed and samples in these aging conditions were tested to fracture in tension at quasi-static strain rates to obtain mechanical data. **Figure 33.6** shows how extending the aging time from 900 s to 1800 s produces an aged condition where the yield stress is nearly equal to that of the TI condition, while maintaining a similar ductility as that of the AQ condition. The characterization of these additional aging treatments has revealed that yield stress is maximized to that obtained in the TI condition before ductility starts to decrease gradually, not sharply to that exhibited in the TI condition. In short, maximum yield stress at near-constant ductility was found to be produced after 1800 s of aging. **Figure 33.7** synthesizes the results and shows the sudden transition and loss of ductility that occurs for aging times past 1800 s.

33A.4 Plans for Next Reporting Period

Future work in this project is aimed in two main thrust areas, consisting of post-mortem characterization and numerical modelling. Post-mortem characterization of the APS dynamic experiment specimens is underway, including EBSD and TEM of all five conditions shown in Table 33.1 for the two different strain rates tested. Modelling efforts are also underway using first principles calculation software "Vienna Ab-Initio Simulation Package" to calculate elastic properties of β Ti binary solid solutions in the composition range where TRIP and TWIP occur during deformation.

33A.5 References

[33.1] C. Brozek, et al., A β-titanium alloy with extra high strain-hardening rate: design and mechanical properties, *Scripta Materialia* 114 (2016): 60-64.

[33.2] F. Sun, et al. A new titanium alloy with a combination of high strength, high strain hardening and improved ductility, *Scripta Materialia* 94 (2015): 17-20.

[33.3] M. Marteleur, et al., On the design of new β-metastable titanium alloys with improved work hardening rate thanks to simultaneous TRIP and TWIP effects, *Scripta Materialia* ,10 (2012): 749-752.

[33.4] X. Min, et al., Mechanism of twinning-induced plasticity in β-type Ti–15Mo alloy, *Scripta Materialia* 69.5 (2013): 393-396.

33A.6 Figures and Tables

Table 33.1 Heat treatment and alloys for APS testing.

Alloys (wt %)	Heat Treatments & Expected Mechanisms		
Ti-10V-2Fe-3Al	As-quenched (AQ) 1123K-0.5h + water quench (WQ) TRIP	Peak-aged AQ+423K-900s TRIP	Over-aged AQ+423K-7200s SLIP
Ti-15Mo	AQ - 800-1h + WQ TWIP		
Ti12-Mo	AQ - 820-1h + WQ TRIP/TWIP		

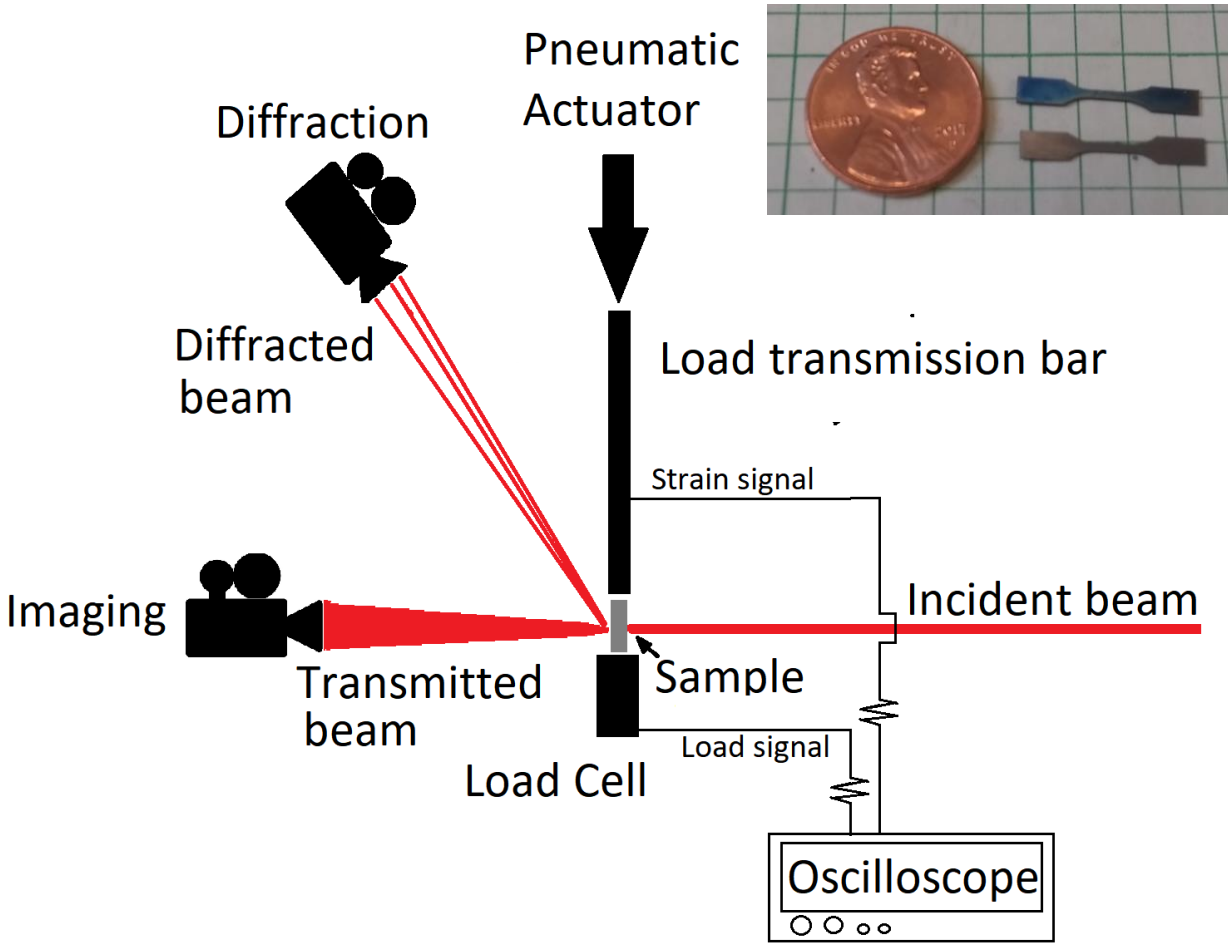

Figure 33A.1 Schematic diagram of the in-situ high-rate testing setup used at the APS beamline 32-ID, showing the concurrent imaging, diffraction and mechanical property measuring capabilities. This system is capable of

testing samples in compression and tension at strain rates of 10^3 s^{-1} or more. The inset image shows an example of a small tensile specimen typically used in this setup next to a penny for scale.

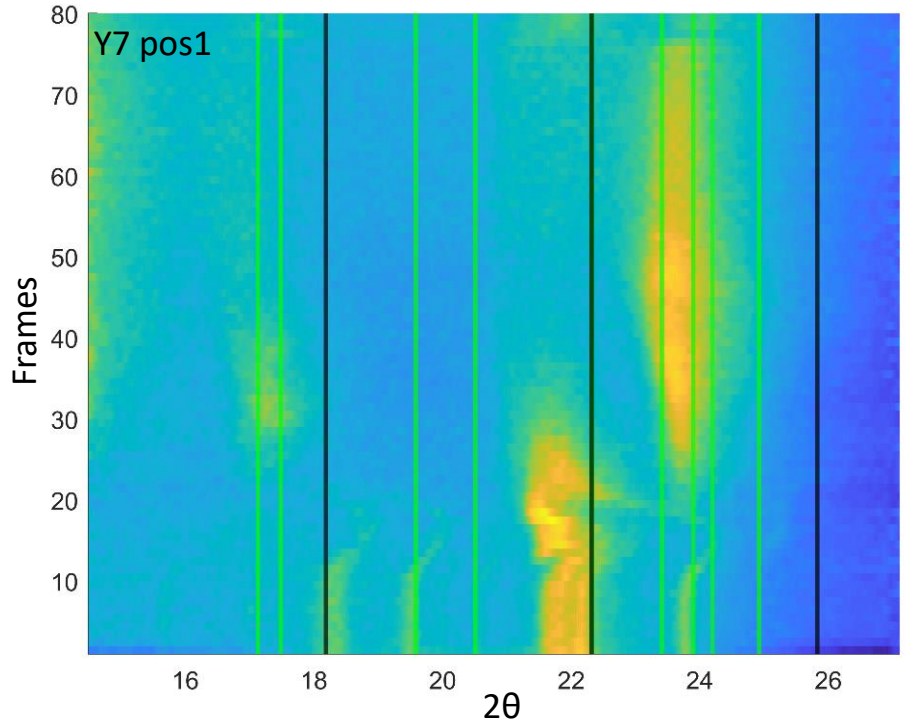

Figure 33A.2: Integrated diffraction pattern of an as-quenched Ti-1023 sample deformed in tension at a strain rate of 10^3 s^{-1} by a pressure bar apparatus at the APS. The vertical lines indicate the theoretical position of diffraction peaks; green is for martensite and black is for β phase. Yielding occurs near frame 30, and fracture occurs near frame 80.

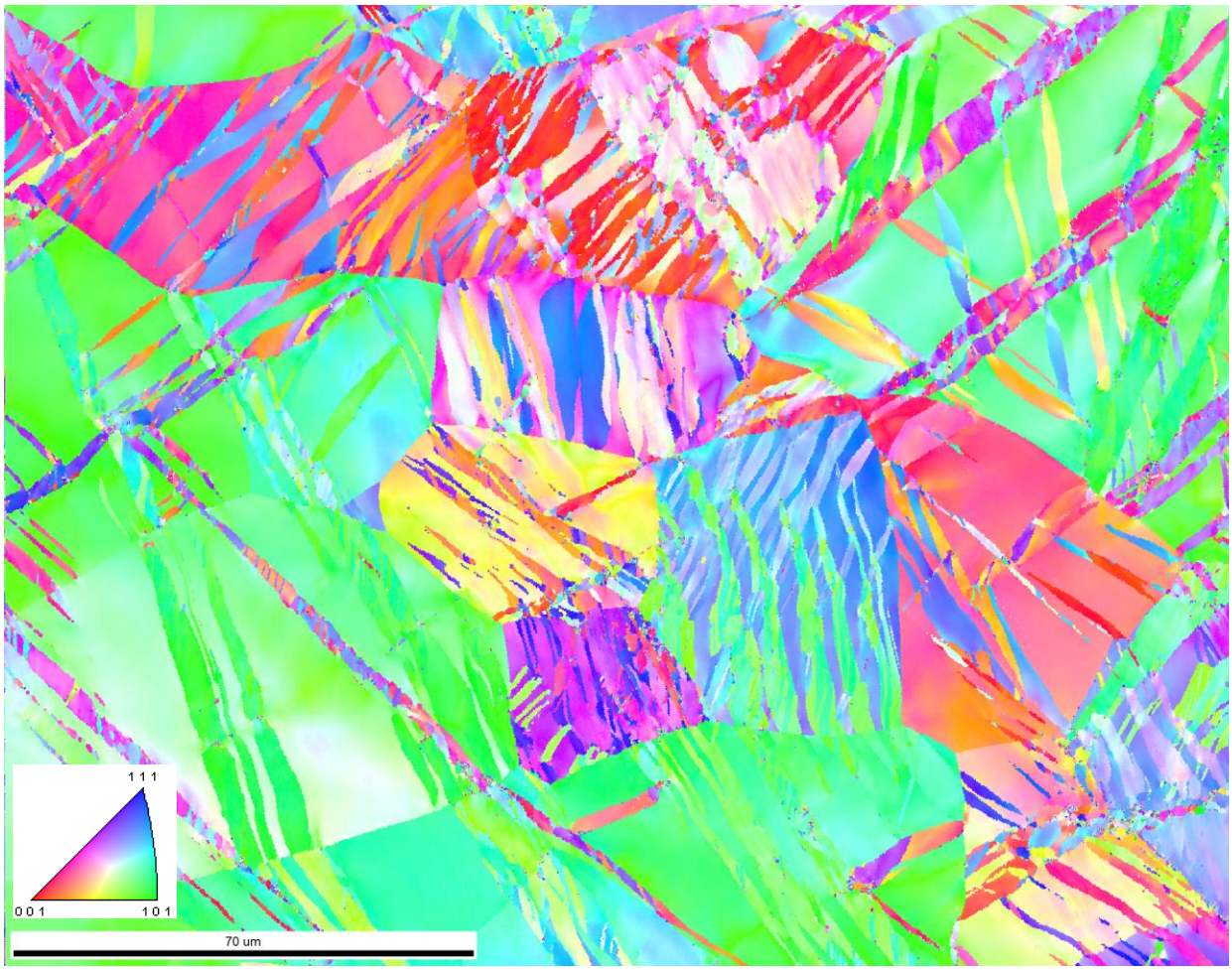

Figure 33A.3: IPF map of a TWIP Ti-15Mo specimen taken from the gage length near the fracture surface. Substantial and complex microstructural evolution has occurred during deformation in the form of primary {332}<113> twinning and secondary twinning on two distinct system : {332}<113> and {112}<111>. A grain dilation cleanup routine was used in OIM software. This sample was tested at a strain rate of 10^3 s^{-1} in tension. The IPF map shows only BCC orientations

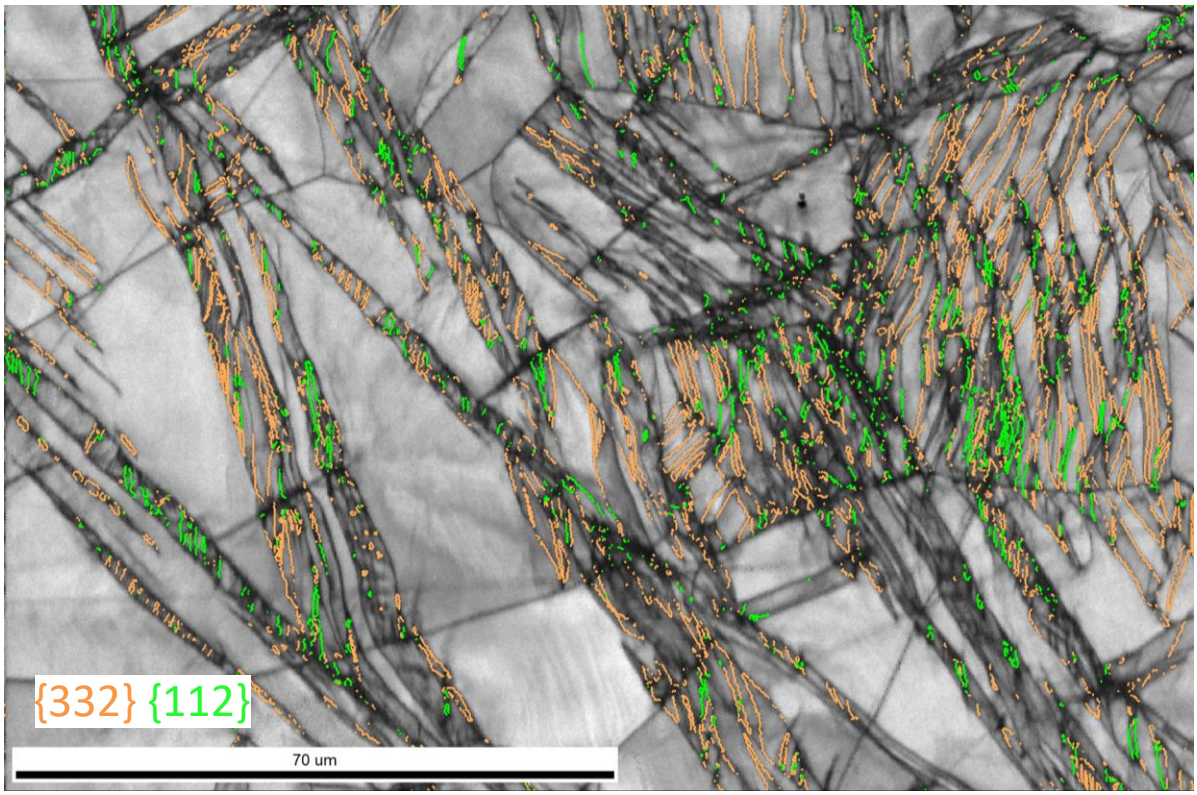

Figure 33A.4: IQ map of a TWIP Ti-15Mo specimen taken from the gage length near the fracture surface. This IQ map is from the same EBSD scan as shown in Figure 33A.4. {332}<113> twin boundaries are highlighted in orange, and {112}<111> boundaries are highlighted in green. This map highlights how {112}<111> twinning seems to from only as a secondary product within the primary {332}<113>, a finding that is unreported in literature.

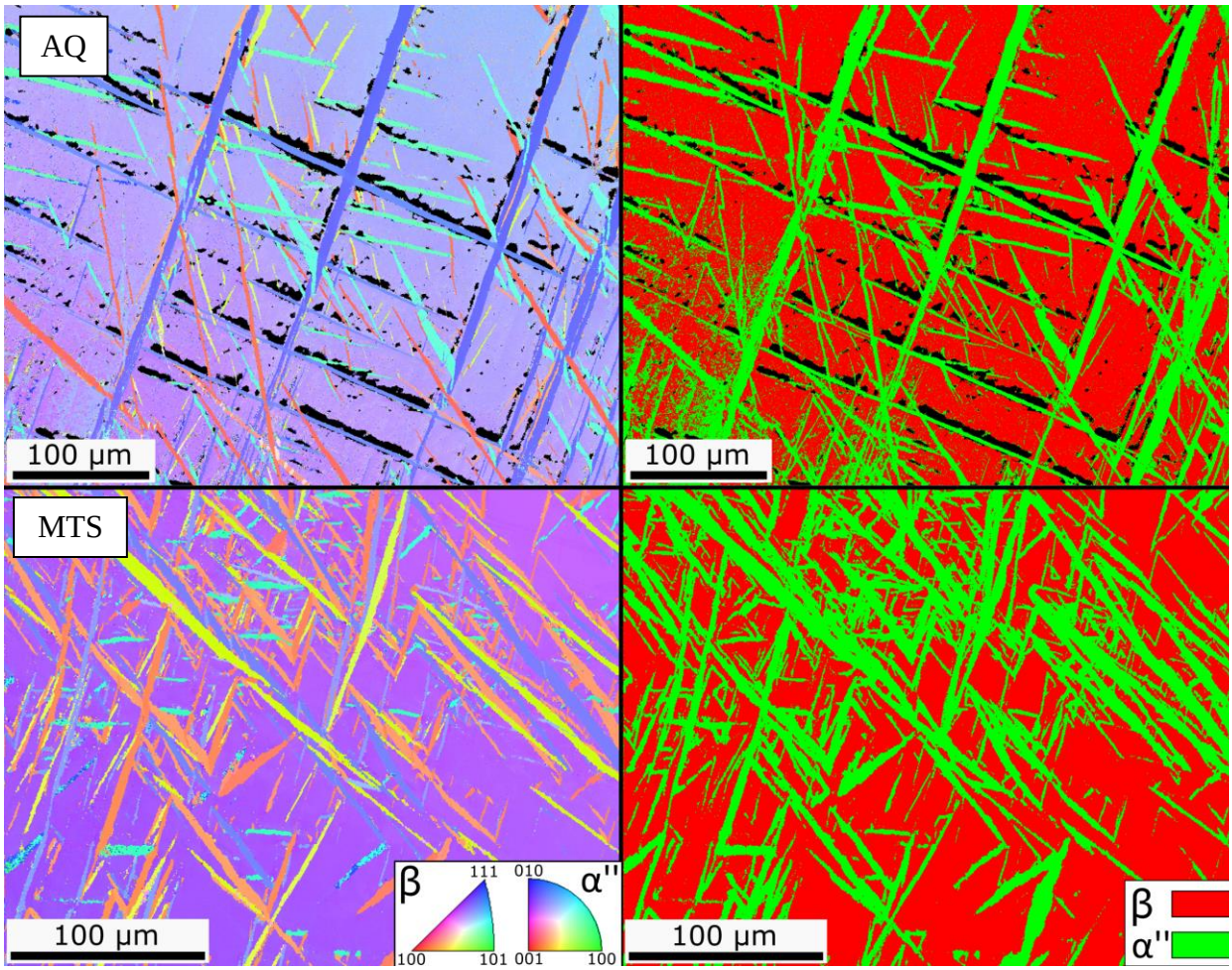

Figure 33A.5: Microstructural evolution revealed in Ti-1023 in 2 aged conditions, namely the AQ and maximum trip stress (MTS) condition, which consists of 900 s of aging at 423 K starting from the AQ condition. EBSD IPF maps and phase maps for the AQ and MTS conditions reveal that the microstructure contains martensite. These scans support the conclusion that deformation in Ti-1023 remains TRIP dominant, even after low-temperature aging.

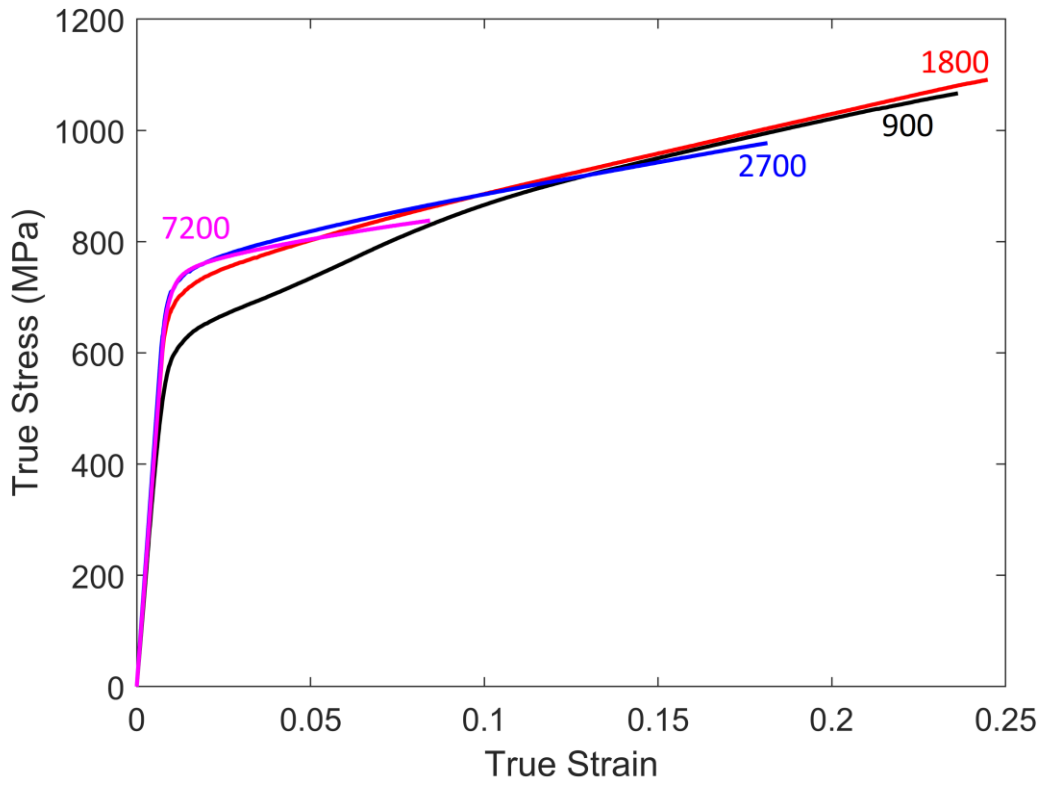

Figure 33A.6 True stress versus true strain plots of Ti-1023 aged at different times and deformed in tension to fracture at quasi-static strain rates. The labels correspond to the numbers of seconds each specimen was aged at 423 K starting from the AQ condition. The 1800 s and 2700 s aged conditions show the transition that occurs from MTS (900 s) to the TI condition (7200 s).

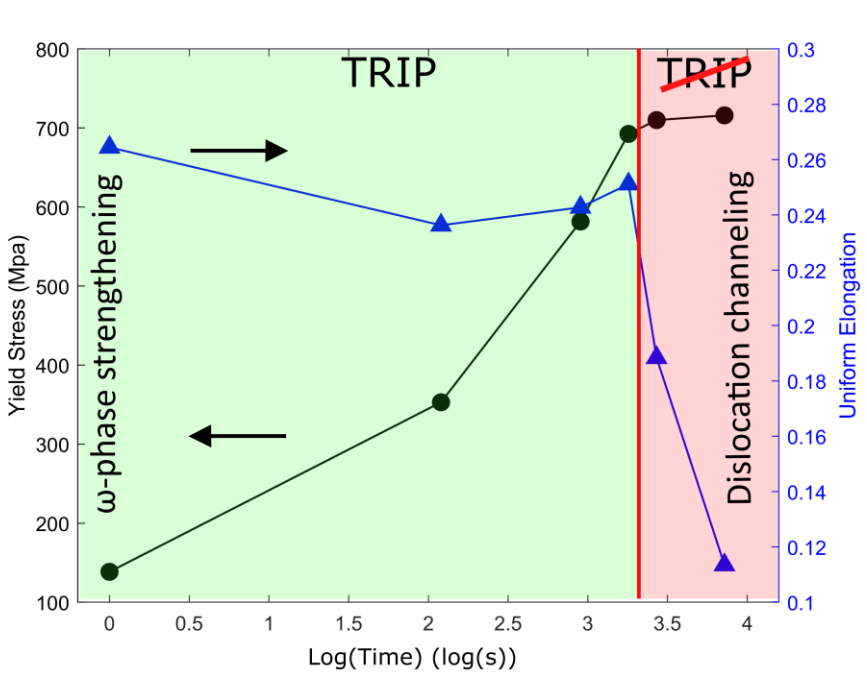

Figure 33A.7: Overview figure showing uniform elongation and yield stress of Ti-1023 deformed in tension at a strain rate of 10^{-3} s^{-1} as a function of aging time on a log scale. Aging time past roughly 1800 s leads to a drastic reduction in ductility, with almost no gain in strength. This data highlights the promising strengthening at near-constant ductility that can be obtained from low-temperature aging.